The 2010 IEEE/RSJ International Conference on
Intelligent Robots and Systems
October 18-22, 2010, Taipei, Taiwan

Experimental Study on Impedance Control for the Five-Finger Dexterous Robot Hand DLR-HIT II

Zhaopeng Chen, Neal Y. Lii, Thomas Wimboeck, Shaowei Fan, Minghe Jin, Christoph H. Borst and Hong Liu

Abstract— **This paper presents experimental results on the five-finger dexterous robot hand DLR-HIT II, with Cartesian impedance control based on joint torque and nonlinearity compensation for elastic dexterous robot joints. To improve the performence of the impedance controller, system parameter estimations with extended kalman filter and gravity compensation have been investigated on the robot hand. Experimental results show that, for the harmonic drive robot hand with joint toruqe feedback, accurate position tracking and stable torque/force response can be achieved with cartesian and joint impedance controller. In addition, a FPGA-based control architecture with flexible communication is proposed to perform the designed impedance controller.**

I. Introduction

In recent years, interest have grown in dexterous robot hand and associated control approaches in robotics. Several anthropomorphic robot hands, such as the NASA Robonaut Hand [1], the DLR Hand II [2] and the DLR-HIT Hand I [3], have been developed as result. However, challenges related to elastic joint based dexterous robot hand's control system remain, such as the lack of an accurate model, high friction, joint flexibility, nonlinearity and uncertain gravity effects [4], [5].

Hogan introduced a framework for impedance control [6], which can be used to achieve compliant manipulation and reliable grasping with different objects in an unknown environments. The goal of Cartesian impedance control is to realize a desired dynamical relationship between the motion of the end-effector and the external forces/torques. Wimboeck et al. developed an object impedance controller for multifinger dexterous manipulation based on passive impedance control on the DLR Hand II [7]. Gonzalez and Widmann proposed a hybrid impedance control scheme, in which a desired force is utilized as the commanded variable, demonstrating enhanced performance with explicit force control structure [8]. Albuschaeffer and Ott [9] [10] [11] [12] implemented Cartesian impedance control with complete static states feedback for DLR LWR arm series (DLR light-weight arms). Asymptotic stability has been proved based on passivity theory.

Zhaopeng Chen, Neal Y. Lii, Thomas Wimboeck, Christoph H. Borst and Hong Liu are with Institute of Robotics and Mechatronics, German Aerospace Center, DLR, 82234 Wessling, Germany zhaopeng.chen@dlr.de

Shaowei Fan, Minghe Jin are with Faculty of State Key Laboratory of Robotics and System, Harbin Institute of Technology, 150001 Harbin, China mhjin_hit0@yahoo.com.cn

Control algorithm for the dexterous robot depends on effective control hardware structure. In order to fulfill requirements including high-speed data transfer, fast calculation, dependable communication and more data/program memory, etc. Field programmable gate array (FPGA) has become a viable option in complex logic circuit design due to its flexibility, ease to use, and short time to market [13]. As shown in [14], the hardware structure of the DLR lightweight robot consists of a DSP/FPGA board in each joint for joint torque controller, a PC-based Cartesian controller and a serial realtime communication specification (SERCOS) based fiber optical bus for communication.

In the above works, nonlinear effects such as friction compensation of the elastic robot joints have only been applied to robot arms, but not explicitly analyzed in robot hand. Therefore, joint and cartesian impedance controller with model-based nonlinear compensation is designed in this paper for the DLR-HIT dextero rous hand II. To overcome the dynamic uncertainties due to approximation in modeling, extended kalman filter is implemented to adaptively estimate parameters for the system dynamics. Furthermore, a DSP/FPGA based mutisensory hardware architecture is proposed to perform the Cartesian impedance control with friction and gravity compensations. The hardware is composed of three DSP/FPGA data processing units, high-speed (200 μs cycle time) multipoint low voltage differential signaling (M-LVDS) serial data bus communicatio system and QNX real-time controller.

This paper is organized as follows: Section II presents the hardware architecture of DSP/FPGA based control system; Section III gives joint and cartesian impedance control architecture of flexible joint dexterous robot; Section IV deals with parameter estimation of system dynamics in detail; experimental results and application are presented in Section V. Finally, the conclusions of this work are drawn and presented in Section VI.

II. Hardware Controller Architecture

Success of robot control system relies not only on the control algorithm, but also on the hardware controller structure. As illustrated in Fig. 1, the proposed control architecture consists of multisensory system, finger controller, palm controller and external real-time controller.

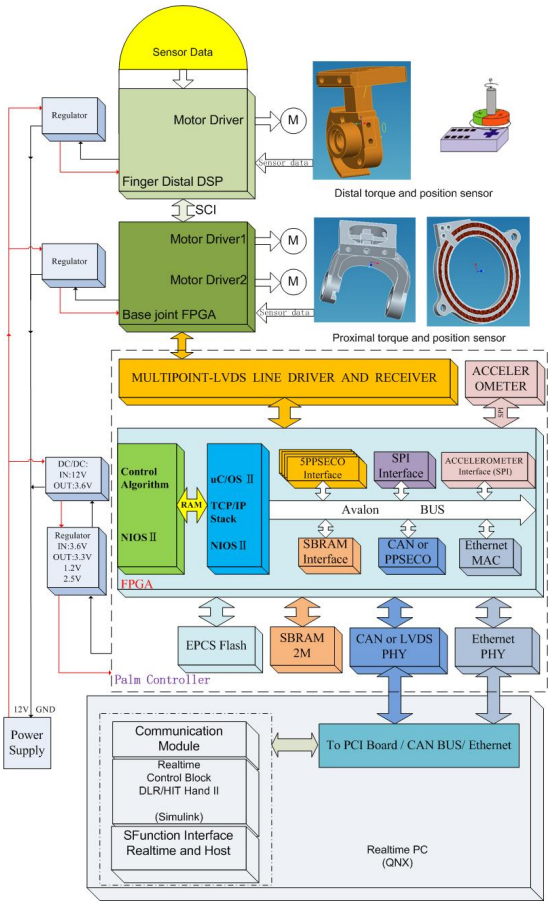

Fig. 1. Controller Diagram

A. Multisensory System

The fingers of the dexterous robot hand DLR-HIT II are identical, which are driven by the BLDC (brushless DC) motor, harmonic drive gear (gear ratio 1:100) and timing belt (ratio 1:1.25). For each finger, two custom designed potentiometers in the proximal joint and a contactless magnetic angle sensor in the finger distal unit are equipped to measure the absolute angular position of the 3 joints. To precisely measure the external torque without any interference between the two DOFs, a new type of proximal joint torque sensor with two DOFs and a distal torque sensor, both based on strain gauge theory, are adopted for the three joints.

B. Hand Controller

For the finger controller, the FPGA provides the processing for the finger base joint motor control, which is physically located at the bottom of a finger base. All the motor driver, communication with finger distal and higher control level, sensor data acquiring are implemented in one single electronic board with Very-High-Speed Integrated Circuit Hardware Description Language (VHDL). Two brushless DC (BLDC) motors are directly driven and controlled by an FPGA with MOSFET driver gates. In order to achieve modularity of the robot finger, all the parameters related to the finger control are stored in the flash memory on the finger base board. The finger distal motor is controlled by a DSP, which is attached on the back side of the first linkage of the finger. For the finger distal motor, a Texas instruments (TI) floating-point digital signal processor (DSP) with maximum 100 MMACS is selected to carry out the sensor signals processing, BLDC motor control, as well as the communication between the finger distal and the finger base.

For the palm controller, a Cyclone III FPGA is chosen with NIOS II dual-processors system implemented in a single chip. With its sufficient processing power, an enhanced controller with more flexible communication system can be achieved in a smaller electronics package. With the advantage of flexible FPGA structure and integrated processing units, the proposed control architecture is able to achieve high control performance in hardware real-time, within a small-sized control hardware electronics. Furthermore, diverse I/O standards support connections between different hardware components (e.g. FPGA, DSP, motor, sensors), which makes the controller more flexible for different applications.

All the Cartesian impedance control algorithm, trajectory planning and dynamic compensation are carried out in a QNX PC with simulink-QNX tool chain, as shown in Fig. 1.

C. Communication System

A large amount of data has to be transmitted between finger controller, palm controller and QNX PC. The data package consists of motor control data, sensor data and tracking data. During communication, the finger controller packs all the digital sensor values, while the palm controller distributes the control signal to each finger, and sends sensor data packages back to the QNX PC at the same time. To realize real-time feedback control of the robot hand, a high speed data bus of M-LVDS is designed and implemented between finger controller, palm controller and QNX PC. And the control cycle time of 200 μs is achieved, which means the control signal and sensor data are updated every 200 μs in real time.

III. Impedance Control for Dexterous Robot Hand

A. Robot Model

The fingers of the dexterous robot hand are of modular design, with identical mechanical structure and control architecture. The joints of the robot fingers are driven by electromechanical hardware, composed of brushless direct-current motors (BLDC) and light weight harmonic drive gears. Flexibility of the joint is inherent its harmonic drive gear, timing belt and the torque sensor. The finger joint impedance control fulfills the requirement between external

force and finger joint position by adjusting the stiffness parameters. The kinematics model of the robot hand with flexible joint [15] is well known, and shown below:

$$M(q)\ddot{q} + C(q,\dot{q})\dot{q} + g(q) = \tau + \tau_{ext} \quad (1)$$

$$B\ddot{\theta} + \tau + \tau_f = \tau_m \quad (2)$$

$$\tau = K(\theta - q) \quad (3)$$

where $M(q) \in \mathbb{R}^{n\times n}$, $C(q) \in \mathbb{R}^n$ and $g(q) \in \mathbb{R}^n$ represent the inertia matrices, centrifugal term, and gravity term, respectively. The joint torque vector is given by $K(\theta - q)$, where θ indicates the vector of the motor angle divided by the gear ratio, and q represents the link side joint angle. K, B are diagonal matrices which contain the joint stiffness, and the motor inertia multiplied by the gear ratio squared. τ_{ext} and τ_f are external torque vector and friction torque vector, respectively. The generalized actuator torque vector, τ_m, is considered as the control input.

B. Joint Level Impedance Control

The goal of the impedance controller is to achieve a desired dynamic behavior with respect to external forces and torques acting on the link side. As shown in Fig. 2, the dynamic behaviour is given by a stiffness parameter K_θ as well as a damping parameter D_θ. Following the idea in [11], interpreting the joint torque feedback as the shaping of the motor inertia makes it possible to use the torque feedback directly within the passivity framework. The controller design is conceptually separated into two steps, one related to torque feedback, and the other to position feedback. Consider a

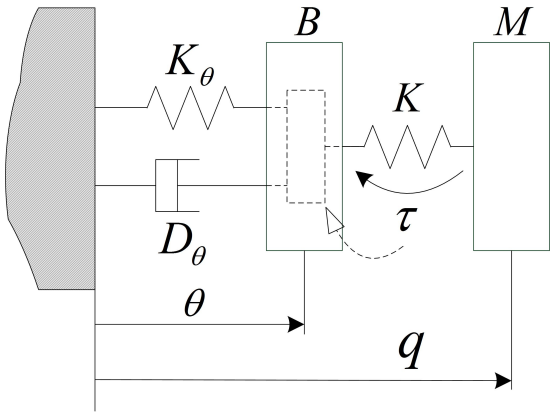

Fig. 2. Model for a Flexible Joint Robot

torque controller of the form:

$$u = \tau + B_\theta \ddot{\theta} \quad (4)$$

where $u \in \mathbb{R}^n$ is a new input variable and B_θ is a diagonal, positive define matrix, such that $b_{\theta i} < b_i$. Then together with (2), the scaling of the apparent rotor inertia from B to B_θ can be achieved by a joint torque feedback:

$$\tau_m = BB_\theta^{-1}u + (I - BB_\theta^{-1})\tau + \tau_f \quad (5)$$

The ratio BB_θ^{-1} for DLR-HIT hand is main determined by the noise level of the torque sensors, values of which should be chosen lower when high stiffness is desired.

For passivity consideration, in case that the desired impedance behavior is defined (w.r.t joint coordinates), a motor position based PD-controller as following can be used:

$$u = -K_\theta(\theta - \theta_s) - D_\theta\dot{\theta} \quad (6)$$

θ_s represents a desired configuration. Together with (2) and (3), the following closed loop equations can be achieved:

$$M(q)\ddot{q} + C(q,\dot{q}) + g(q) = \tau + \tau_{ext} \quad (7)$$

$$B_\theta\ddot{\theta} + D_\theta\dot{\theta} + K_\theta\tilde{\theta} + \tau + B_\theta B^{-1}\tau_f = 0 \quad (8)$$

where $\tilde{\theta} = \theta - \theta_s$.

C. Cartesian Level Impedance Control

In the following, it is assumed that the position and orientation of the end-effector can be described by a set of local coordinates $x \in \mathbb{R}^m$, and the relationship between Cartesian coordinates x and the configuration coordinates $q \in \mathcal{Q}$ is given by a known function $f : \mathcal{Q} \to \mathbb{R}^m$, i.e. $x = f(q)$. As described in [16], with the Jacobian $J(q) = \partial f(q)/\partial q$, Cartesian velocities and accelerations can be written as

$$\dot{x} = J(q)\dot{q} \quad (9)$$

$$\ddot{x} = J(q)\ddot{q} + \dot{J}(q)\dot{q} \quad (10)$$

Throughout this paper only the nonsingular case is considered, thus it is assumed that the manipulator's Jacobian $J(q)$ has full row rank in the considered region of the workspace.

To specify the desired impedance behavior, the position error $\tilde{x} = x - x_d$, between real position x and a virtual equilibrium position (possibly time-varying) x_d, is introduced. The goal of the impedance controller here is to alter the system dynamics (1) such that, in the presence of external forces and torques at the end-effector $F_{ext} \in \mathbb{R}^m$, a dynamic relationship between $\tilde{x}$ and F_{ext} could be achieved as follows:

$$\Lambda_d\ddot{\tilde{x}} + D_d\dot{\tilde{x}} + K_d\tilde{x} = F_{ext} \quad (11)$$

where Λ_d, D_d and K_d are the symmetric and positive definite matrices of the desired inertia, damping and stiffness, respectively.

The relationship between the external torque vector τ_{ext} and the generalized external force vector F_{ext} on the end-effector is given by:

$$\tau_{ext} = J(q)^T F_{ext} \quad (12)$$

Substituting $\ddot{q} = J(q)^{-1}(\ddot{x} - \dot{J}(q))\dot{q}$ From (10) and (12) into (1) leads to

$$M(q)J(q)^{-1}(\ddot{x} - \dot{J}(q)\dot{q}) + C(q,\dot{q})\dot{q} + g(q) = \tau + J(q)^T F_{ext} \quad (13)$$

With $\dot{q} = J(q)^{-1}\dot{x}$ from (9) and by pre-multiplying the resulting equation by $J(q)^{-T}$, the relationship between the Cartesian coordinates x and the joint torques τ can now be expressed in the form:

$$\Lambda(x)\ddot{x} + \mu(x,\dot{x}) + J(q)^{-T}g(q) = J(q)^{-T}\tau + F_{ext} \quad (14)$$

where the matrices $\Lambda(x)$ and $\mu(x,\dot{x})$ are given by:

$$\Lambda(x) = J(q)^{-T}M(q)J(q)^{-1} \quad (15)$$

$$\mu(x,\dot{x}) = J(q)^{-T}(C(q,\dot{q}) - M(q)J(q)^{-1}\dot{J}(q))J(q)^{-1} \quad (16)$$

with $q = f^{-1}(x)$ and $\dot{q} = J(f^{-1}(x))\dot{x}$.

By treating them as the external torques, the gravity torque $g(q)$ and the joint torque τ can be rewritten in form of the equivalent task space gravity forces $F_g(x)$ and the new input vector F_τ. Therefore, the system equations can be expressed in the form:

$$\Lambda(x)\ddot{x} + \mu(x,\dot{x})\dot{x} + F_g(x) = F_\tau + F_{ext} \quad (17)$$

$\Lambda(x)$ and $\mu(x,\dot{x})$ are the inertia matrix and the Coriolis/centrifugal matrix with respect to the coordinates x. Combining (17) and (11), the impedance control law, which is the desired closed loop system, with F_τ as the control input, can be arrived:

$$F_\tau = \Lambda(x)\ddot{x}_d + \mu(x,\dot{x})\dot{x} + (\Lambda(x)\Lambda_d^{-1} - I)F_{ext} - F_g(x) - \Lambda(x)\Lambda_d^{-1}(D_d\dot{\tilde{x}} + K_d\tilde{x}) \quad (18)$$

If the desired torque vector τ is chosen as:

$$\tau = J(q)^T F_\tau + C(q,\dot{q})\dot{q} - J(q)^T\Lambda(x)\dot{J}(q)J(q)^{-1} \quad (19)$$

(18) can be simplified as:

$$F_\tau = \Lambda(x)\ddot{x}_d - \Lambda(x)\Lambda_d^{-1}(D_d\dot{\tilde{x}} + K_d\tilde{x}) + F_g(x) + (\Lambda(x)\Lambda_d^{-1} - I)F_{ext} \quad (20)$$

With the assumption that centripetal and Coriolis forces can be ignored at the robot's relatively low operating speeds (with maximal velocity $0.3m/s$ for the DLR-HIT robot hand). Furthermore, If the desired inertia Λ_d is chosen as identical to the robot inertia $\Lambda(x)$, the feedback of external forces F_{ext} can be avoided. Then it follows that actual implementation of the impedance controller:

$$F_\tau = \Lambda(x)\ddot{x}_d - D_d\dot{\tilde{x}} - K_d\tilde{x} + F_g(x) \quad (21)$$

then follows the desired joint torques τ:

$$\tau = g(q) + J(q)^T(\Lambda(x)\ddot{x}_d - D_d\dot{\tilde{x}} - K_d\tilde{x}) \quad (22)$$

Using motor θ instead of the link side angles q in the forward kinematics $x = f(q)$, impedance controller based on PD position control w.r.t Cartesian coordinates can be generalized from (6). Then the feedback law is given by:

$$\begin{aligned} u &= -J(\theta)^T(K_x\tilde{x}(\theta) + D_x\dot{x}) \\ \tilde{x}(\theta) &= f(\theta) - x_d \\ \dot{x} &= J(\theta)\dot{\theta} \end{aligned} \quad (23)$$

with K_x and D_x represent the desired stiffness and damping matrices, respectively corresponding to K_d and D_d in (22). x_d indicates the virtual motor side position in Cartesian coordinates. The the controller in (23), together with (5), forms the closed loop system:

$$\begin{aligned} M(q)\ddot{q} + C(q,\dot{q}) + g(q) &= \tau + \tau_{ext} \\ B_\theta\ddot{\theta} + J(\theta)^T(K_x\tilde{x}(\theta) + D_x\dot{x}) + \tau &= 0 \end{aligned} \quad (24)$$

IV. Dexterous Robot Hand Dynamics

A. Gravity Compensation

As shown in [17], the gravity torque compensation term in the desired steady state can be used for a motor position based PD-controller. For the DLR-HIT II dexterous robot hand, the gravity compensation is realized with the nominal parameters of the robot (D-H parameters and masses, etc.), shown in Fig. 3. The gravity forces on the robot hand can be written as:

$$\begin{aligned} g(\theta) &= \frac{\partial V(\theta)}{\partial\theta} \\ V(\theta) &= m_2gh_2(\theta) + m_3gh_3(\theta) + m_4gh_4(\theta) \end{aligned} \quad (25)$$

where V is the potential energy of the robot hand. m_i and h_i represent the mass of each joint and the height of the mass center respectively, which can be obtained by using the forward kinematics map.

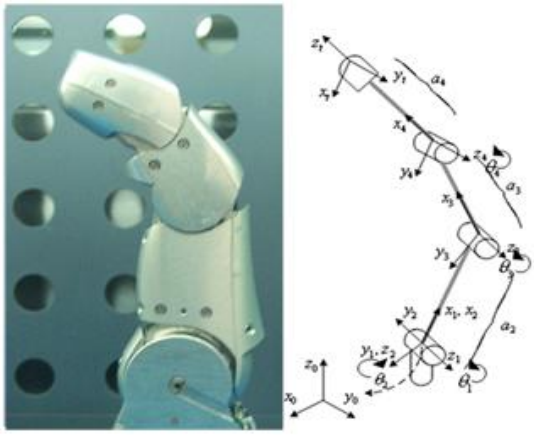

Fig. 3. Dexterous Robot Hand and Reference Frame

In case of an impedance controller, however, large deviations from the steady state positions may occur in case of a

small desired stiffness. Ott constructed a compensation term, which relies solely on the motor position, and is able to compensate for the link side gravity torques [9]. Consider the set $\boldsymbol{\Omega} := \{(q,\theta)|K(\theta - q) = g(q)\}$ of stationary points (for $\tau_{ext} = \mathbf{0}$), the goal of the gravity compensation is now to construct a compensation term $\bar{g}(\theta)$ such that in $\boldsymbol{\Omega}$:

$$\bar{g}(\theta) = g(q) \quad \forall (q,\theta) \in \boldsymbol{\Omega} \tag{26}$$

which can be carried out by the computable relationship between θ and q. Notice that for any point $(\theta, q) \in \boldsymbol{\Omega}$, the motor position can be expressed uniquely as a function of the link side position:

$$\theta = q + K^{-1} g(q) := h(q) \tag{27}$$

Furthemore, it is shown in [9] that the inverse function to $h(q)$ exists, and the mapping $T(q) := \theta - K^{-1} g(q)$ is a contraction. Thus the iteration:

$$\begin{aligned} \hat{q}_{n+1} &= T(\hat{q}_n) \\ &= \theta - K^{-1} g(\hat{q}_n) \end{aligned} \tag{28}$$

converges for every starting point, as follows from the contraction mapping theorem [18]. By using $\hat{q}_0 = q_s$ one would obtain satisfactory gravity compensation with one or two iteration steps [19].

B. Velocity Observer and Friction Compensation

The performance of the controller can be significantly improved with appropriate robot dynamic model. A model with viscous and static friction is chosen in this paper, which is described as:

$$\tau_f = b\dot{\theta} + csign(\dot{\theta}) \tag{29}$$

b and c are viscous friction coefficient and static friction coefficient, respectively. The dynamic model of the robot system is expressed as:

$$I\ddot{\theta} = \tau - b\dot{\theta} - csgn(\dot{\theta}) \tag{30}$$

where $\tau = \tau_m - \tau_{ext}$, I represents motor inertia. In order to implement controller with friction compensation, it is necessary to determine parameters corresponding to the robot dynamical model. Kalman filter is a powerful estimation approach when the precise nature of the modeled system is unknown, which can be used to fulfill the nonlinear system parameter estimation for DLR-HIT dexterous hand II. The proposed controller design with extended Kalman filter is described in this section.

The extended Kalman filter is subdivided into prediction step and estimation step as shown in [20]. Based on the current state and the dynamic model of the system, a forecast can be calculated for the state in the prediction step:

$$\begin{aligned} \Delta\hat{x}_{k+1}^{-} &= A_k \Delta\hat{x}_k^{+} + B_K u_k \\ P_{k+1}^{-} &= A_k P_k^{+} + G_K Q_k G_k^T \end{aligned} \tag{31}$$

The estimation step is defined, where the forecast and the measurements are compared, and an optimal compromise is made:

$$\begin{aligned} K_k &= P_k^{-} H_k^T (H_k P_k^{-} H_k^T + R_k)^{-1} \\ \Delta\hat{x}_k^{+} &= \Delta\hat{x}_k^{-} - K(H_k \Delta\hat{x}_k^{-} - \Delta y_k) \\ P_k^{+} &= (I - K_k H_k) P_k^{-} \end{aligned} \tag{32}$$

In order to eliminate a possible divergence of Δx, the error state is set accordingly to zero after the estimation step.

As described in [21], to derive an adaptive Kalman filter, viscous and static friction parameters b and c are modeled as constant system states. τ is considered as a state variable, or specifically a measurement variable rather than an input variable. The influence of τ can be adjusted by tuning its corresponding system noise parameter. Then the dynamic model of the system can be expressed as :

$$\underbrace{\frac{d}{dt}\begin{pmatrix} \theta \\ \dot{\theta} \\ \tau \\ b \\ c \end{pmatrix}}_{:=x} = \underbrace{\begin{pmatrix} \dot{\theta} \\ \frac{1}{I}(\tau - b\dot{\theta} - csign(\dot{\theta})) \\ 0 \\ 0 \\ 0 \end{pmatrix}}_{:=a} \tag{33}$$

The parameters describing viscous and static friction are estimated along with position, velocity and τ. Therefore further nonlinearities besides the ones already mentioned are introduced into the system. By partial deriving the system dynamics equation, replacing the partial derivation sign ∂ with differences sign Δ and using linearlized form of sign function:

$$f(\dot{\theta}) = \begin{cases} -1 & \dot{\theta} < -limit \\ \frac{1}{limit} & -limit < \dot{\theta} < limit \\ 1 & limit < \dot{\theta} \end{cases}$$

where nonlinearities in the system dynamic model can be eliminated. The following linearized system dynamics equation can be arrived:

$$\frac{d}{dt}\begin{pmatrix} \Delta\theta \\ \Delta\dot{\theta} \\ \Delta\tau \\ \Delta b \\ \Delta c \end{pmatrix} = A_{lin} \cdot \begin{pmatrix} \Delta\theta \\ \Delta\dot{\theta} \\ \Delta\tau \\ \Delta b \\ \Delta c \end{pmatrix} \tag{34}$$

where:

$$A_{lin} = \begin{pmatrix} 0 & 1 & 0 & 0 & 0 \\ 0 & -(\frac{b}{I} + \alpha\frac{c}{I}) & \frac{1}{I} & \frac{-\dot{\theta}}{I} & \frac{-f(\dot{\theta})}{I} \\ 0 & 0 & 1 & 0 & 0 \\ 0 & 0 & 0 & 1 & 0 \\ 0 & 0 & 0 & 0 & 1 \end{pmatrix} \tag{35}$$

with α represents the derivation of $f(\dot{\theta})$, given by:

$$\alpha = \begin{cases} 0 & \dot{\theta} < -limit \\ \frac{1}{limit} & -limit < \dot{\theta} < limit \\ 0 & limit < \dot{\theta} \end{cases}$$

Solution to the differential equations (34) can be expressed [22] as:

$$\begin{aligned} \boldsymbol{X(t)} &= \boldsymbol{\Phi(t,t_0)\cdot X(t_0)} \\ \boldsymbol{\Phi(t,t_0)} &= \boldsymbol{e^{A_{lin}(t-t_0)}} \end{aligned} \tag{36}$$

The discrete-time-space solution is achieved by calculating (36) from discrete time $\boldsymbol{k\cdot t_s}$ to $\boldsymbol{(k+1)\cdot t_s}$ and expanding the exponential function in its power series:

$$\begin{aligned} \boldsymbol{X_{k+1}} &= \boldsymbol{A_k \cdot X_k} \\ \boldsymbol{A_k} &= \boldsymbol{1 + A_{lin,k}\cdot\frac{t_s}{1!} + A_{lin,k}^2\cdot\frac{t_s}{2!}+\cdots} \end{aligned} \tag{37}$$

where $\boldsymbol{A_{lin,k} = A_{lin}(x(kt_s)) = A_{lin}}$. Together with (35), the linearized adaptive kalman filter results in:

$$\boldsymbol{\Delta x_{k+1}} = \begin{pmatrix} \boldsymbol{1} & \boldsymbol{a_2} & \boldsymbol{a_3} & \boldsymbol{-\dot\theta\cdot a_3} & \boldsymbol{-f(\dot\theta)\cdot a_3} \\ \boldsymbol{0} & \boldsymbol{a_1} & \boldsymbol{\frac{1}{I}\cdot a_2} & \boldsymbol{-\frac{\dot\theta}{I}\cdot a_2} & \boldsymbol{-\frac{f(\dot\theta)}{I}\cdot a_2} \\ \boldsymbol{0} & \boldsymbol{0} & \boldsymbol{1} & \boldsymbol{0} & \boldsymbol{0} \\ \boldsymbol{0} & \boldsymbol{0} & \boldsymbol{0} & \boldsymbol{1} & \boldsymbol{0} \\ \boldsymbol{0} & \boldsymbol{0} & \boldsymbol{0} & \boldsymbol{0} & \boldsymbol{1} \end{pmatrix} \cdot \boldsymbol{\Delta x_k} \tag{38}$$

Where:

$$\begin{aligned} \boldsymbol{a_1} &= \boldsymbol{e^{-(b+\alpha c)\cdot\frac{t_s}{I}}} \\ \boldsymbol{a_2} &= \boldsymbol{\frac{I}{b+\alpha c}\cdot(1-e^{-(b+\alpha c)\cdot\frac{t_s}{I}})} \\ \boldsymbol{a_3} &= \boldsymbol{\frac{I}{(b+\alpha c)^2}\cdot(e^{-(b+\alpha c)\cdot\frac{t_s}{I}} - 1 + (b+\alpha c)\frac{t_s}{I})} \end{aligned}$$

Fig. 4 illustrates the experimental results of viscous and static friction parameters estimated with extended Kalman filter. The estimations converge towards the assumed values ($\boldsymbol{b = 0.3}$, $\boldsymbol{c = 0.2}$) calculated with the least-squares technique as shown in the figure, which indicates the effectiveness of the proposed Kalman filter. The consistent errors, especially with the estimation of c, can be explained with the necessary approximations and linearizations during the filter-design. The system noise $\boldsymbol{Q}$ and the measurement noise covariance $\boldsymbol{R}$ play a crucial role in the performance of the Kalman filter. Superior filter performance can be obtained by tuning the filter parameters $\boldsymbol{Q}$ and $\boldsymbol{R}$ offline. The behavior of the Kalman filter can also be observed in the velocity estimation, as shown in Fig. 5.

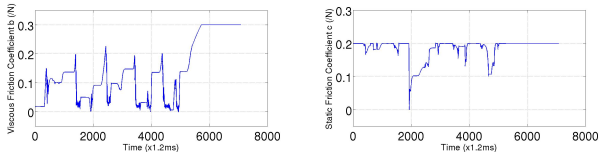

(a) viscous fricition parameter b (b) static fricition parameter c

Fig. 4. Friction Parameter Estimation with EKF

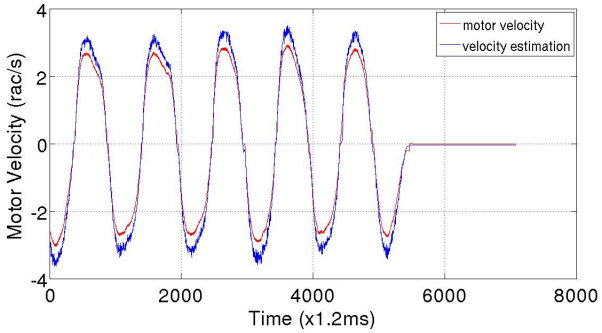

Fig. 5. Velocity Estimation with EKF

V. Experiments and Grasping Application

A. Joint Impedance Control

In this experiment, each joint of the finger is independently driven. The aim is to make all three joints of the finger move in different direction, coming in contact with an external object before reaching the desired position. Damping and stiffness are set at $\boldsymbol{D_d = [0.0013, 0.0013, 0.0031](N\cdot m\cdot s/^\circ)}$, $\boldsymbol{K_d = [0.0625, 0.0625, 0.125](N\cdot m/^\circ)}$. Fig. 7 shows all the finger joints tracking the desired position trajectory (red dash line). As shown in Fig. 6, contact is made with a rigid external object at joint angles of $\boldsymbol{[28^\circ, 52^\circ, 17.5^\circ]}$ (distal, proximal and abduct joint respectively), where real tracking seperates from the desired tracking. The experimental results show that the joints can follow the desired trajectory closely in the free space, and the joints torque increases stably while they make contact with the environment. It can therefore be concluded that the finger joint space impedance control behavior is successfully achieved.

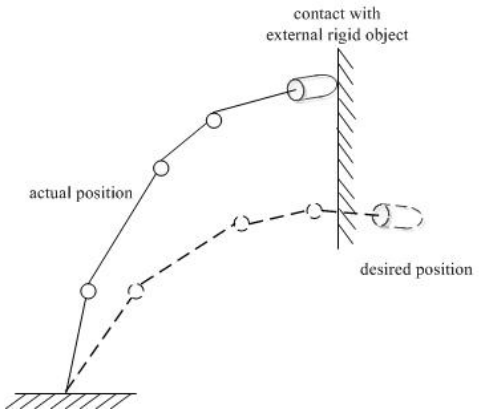

Fig. 6. Robot Finger Contacts with External Rigid Object

B. Cartesian Impedance Control

For the cartesian impedance control law (20)-(24), the following control parameters $\boldsymbol{\Lambda(x)}$, $\boldsymbol{g(\bar x)}$, $\boldsymbol{K_x}$ and $\boldsymbol{D_x}$

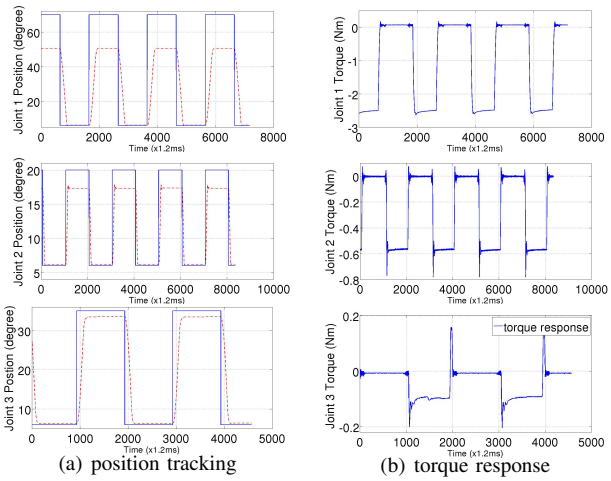

(a) position tracking (b) torque response

Fig. 7. Position Tracking and Force Response in Three Joints of the Finger

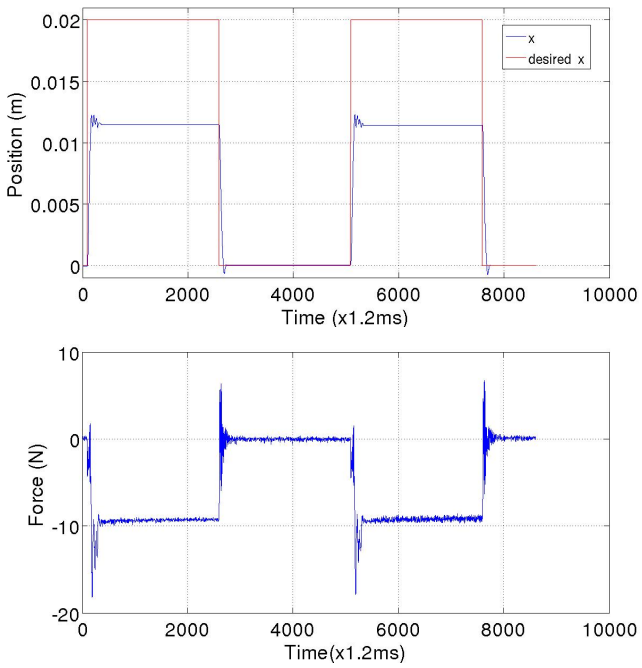

Fig. 8. Cartesian Position and Force Tracking with Contacting Evironment

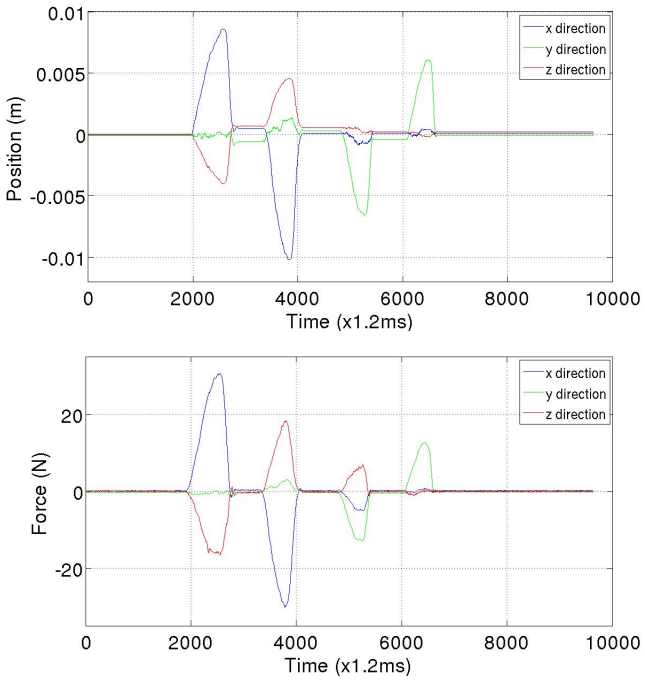

Fig. 9. Cartesian Coordinate Varies and Torque Response with External Force

should be known. As described in Section IV, $\boldsymbol{g}(\bar{\boldsymbol{x}})$ as well as $\boldsymbol{\Lambda}(\boldsymbol{x})$ can be generated by directly using Pro/E model of the dexterous hand. $\boldsymbol{D_x}$ and $\boldsymbol{K_k}$ are designed by the double-diagonalization appoach with the robot inertia matrix and the desired damping ratio, as presented in [10].

The cartesian impedance control experiment has been made in the single finger of the robot hand with the other finger are braked. As shown in Fig. 8, the joint tracks the desired position trajectory(red line), with real tracking curve is shown as the solid line, and contacts a rigid environment where the position offset $\boldsymbol{\Delta x} = \boldsymbol{0.0115m}$ in $\boldsymbol{x}$ direction. The filtered joint torque can also be found in Fig. 8 and. The experiment results show that the joint can follow the desired trajectory closely in the free space, and the joint torque increases stably while it makes contact with the environment.

In a further experiment, the robot pauses at an virtual equilibrium position $\boldsymbol{x_d} = [\boldsymbol{0.036, 0.036, 0.2}]$ w.r.t cartesian coordinates. And we pull the endpoint of the finger in different direction and then release the finger. Fig. 9 illustrate the corresponding Cartesian position offset varies and forces along with the Cartesian position with the proposed Cartesian impedance controller. The robot overcomes the gravity and friction, returning to the $\boldsymbol{x_d}$ as soon as the external force is released. With friction and gravity compensation proposed in this paper, the static error in the $\boldsymbol{x}$ axis is less than 0.2 mm, as well as $\boldsymbol{y}$ and $\boldsymbol{z}$ direction. It can therefore be concluded that the Cartesian impedance behavior is successfully achieved.

VI. Conclusions and Future Work

In this paper, an impedance controller for dexterous robot hand with elastic joints is derived in both Cartesian space and joint space. Gravity compensation based on motor angle is implemented to compensate the link side gravity. The model-based friction estimation and velocity observer are carried out with an extended Kalman filter, which is implemented to adaptively handle parameter uncertainties. The designed estimator demonstrates good prediction performance, as shown in the experimental results. A DSP/FPGA hardware structure with multisensory system and real-time communication is designed for the practical implementation of the proposed

controller. Impedance control experiments are conducted with five-finger dexterous robot hand DLR-HIT II in joint and Cartesian coordinate systems, which show the effectiveness of the proposed controller and hardware architecture.

Successful implementation of Cartesian impedance controller paves the way for designing object level impedance control, while hand-arm telemanipulation systems [23] together with exoskeleton can be carried out based on the proposed joint space impedance controller. The Friction observer and stability analysis of the impedance controller with friction compensation should be further investigated to help improve compensation performance, and therefore impedance control behavior. Hand grasping application and two-hand manipulation with DLR-HIT II dexterous robot hands will also be explored in the future.

REFERENCES

[1] C. Lovchik and M. Difler, "The robonaut hand: A dextrous robotic hand for space," in *Proceedings of the IEEE International Conference on Robotics and Automation*, 1999, pp. 907–912.

[2] J. Butterfass, M. Grebenstein, and H. Liu, "DLR-Hand II: Next generation of a dexterous robot hand," in *Proceedings of the 2001 IEEE International conference on Robotics & Automation*, 2001, pp. 109–114.

[3] R. Wei, X. Gao, M. Jin, Y. Liu, H. Liu, N. Seitz, R. Gruber, and G. Hirzinger, "FPGA based hardware architecture for HIT/DLR hand," in *2005 IEEE/RSJ International Conference on Intelligent Robots and Systems, 2005.(IROS 2005)*, 2005, pp. 523–528.

[4] C. Kennedy and J. Desai, "Modeling and control of the Mitsubishi PA-10 robot arm," *IEEE/ASME Transactions on Mechatronics Transactions*, vol. 10, no. 3, pp. 263–74, 2005.

[5] N. Kircanski and A. Goldenberg, "An experimental study of nonlinear stiffness, hysteresis, and friction effects in robot joints with harmonic drives and torque sensors," *The International Journal of Robotics Research*, vol. 16, no. 2, p. 214, 1997.

[6] N. Hogan, "Impedance control-An approach to manipulation. I-Theory. II-Implementation. III-Applications," *ASME, Transactions, Journal of Dynamic Systems, Measurement, and Control (ISSN 0022-0434)*, vol. 107, 1985.

[7] T. Wimboeck, C. Ott, and G. Hirzinger, "Passivity-based object-level impedance control for a multifingered hand," in *IEEE/RSJ International Conference on Intelligent Robots and Systems*, 2006, pp. 4621–4627.

[8] J. Gonzalez and G. Widmann, "A force commanded impedance control scheme for robots with hardnonlinearities," *IEEE Transactions on Control Systems Technology*, vol. 3, no. 4, pp. 398–408, 1995.

[9] C. Ott, A. Albu-Schaeffer, A. Kugi, S. Stramigioli, and G. Hirzinger, "A passivity based Cartesian impedance controller for flexible joint robots–Part I: torque feedback and gravity compensation," in *IEEE International Conference on Robotics and Automation*. Citeseer, 2004, pp. 2659–65.

[10] A. Albu-Schaeffer, C. Ott, and G. Hirzinger, "A passivity based Cartesian impedance controller for flexible joint robots–Part II: full state feedback, impedance design and experiments," in *IEEE International Conference on Robotics and Automation*. Citeseer, 2004, pp. 2666–2672.

[11] A. Albu-Schaeffer, C. Ott, and G. Hirzinger, "A unified passivity-based control framework for position, torque and impedance control of flexible joint robots," *The International Journal of Robotics Research*, vol. 26, no. 1, pp. 5–21, 2007.

[12] C. Ott, A. Albu-Schaeffer, A. Kugi, and G. Hirzinger, "On the Passivity-Based Impedance Control of Flexible Joint Robots," *IEEE Transactions on Robotics*, vol. 24, no. 2, pp. 416–429, 2008.

[13] J. Huang, Z. Xie, H. Liu, K. Sun, Y. Liu, and Z. Jiang, "DSP/FPGA-based Controller Architecture for Flexible Joint Robot with Enhanced Impedance Performance," *Journal of Intelligent and Robotic Systems*, vol. 53, no. 3, pp. 247–261, 2008.

[14] G. Hirzinger and I. Schaefer, "Space robotics-driver for a new mechatronic generation of light-weight arms," in *IEEE/ASME Iternational Conference on Advanced Intellgent Mechatronics Proceedings*, 2001.

[15] M. Spong, "Modeling and Control of Elastic Joint Robots," *Journal of Dynamic Systems, Measurement, and Control*, vol. 109, p. 310, 1987.

[16] C. Ott, *Cartesian impedance control of redundant and flexible-joint robots*. Springer Verlag, 2008.

[17] P. Tomei, "A simple PD controller for robots with elastic joints," *IEEE Transactions on Automatic Control*, vol. 36, no. 10, pp. 1208–1213, 1991.

[18] M. Vidyasagar, *Nonlinear systems analysis*. Society for Industrial Mathematics, 2002.

[19] L. Zollo, B. Siciliano, A. De Luca, E. Guglielmelli, and P. Dario, "Compliance control for a robot with elastic joints," in *IEEE Intern. Conf. on Advanced Robotics*, 2003, pp. 1411–1416.

[20] A. Gelb, *Applied optimal estimation*. MIT press, 2002.

[21] C. P. Connette, *Intern Report On DLR Hand II*. Institute of Robotic and Mechatronics, DLR, 2006.

[22] R. Brown and P. Hwang, *Introduction to random signals and applied Kalman filtering*. Wiley New York, 1992.

[23] N. Y. Lii, Z. Chen, P. Benedikt, C. H. Borst, G. Hirzinger, and A. Schiele, "Toward Undertanding the Effects of Visual- and Force-Feedback on Robotic Hand Grasping Performance for Space Teleoperation," in *IEEE/RSJ International Conference on Intelligent Robots and Systems (accepted)*, 2010.